Spectral computation of low probability tails for the homogeneous Boltzmann equation

John Zweck[a,*], Yanping Chen[a], Matthew J. Goeckner[b], Yannan Shen[c]

[a] *Department of Mathematical Sciences, The University of Texas at Dallas, Richardson, TX 75080, USA*

[b] *Department of Physics, The University of Texas at Dallas, Richardson, TX 75080, USA*

[c] *Department of Mathematics, University of Kansas, Lawrence, KS 66045, USA*

Abstract

We apply the spectral-Lagrangian method of Gamba and Tharkabhushanam for solving the homogeneous Boltzmann equation to compute the low probability tails of the velocity distribution function, f, of a particle species. This method is based on a truncation, $Q^{\rm tr}(f,f)$, of the Boltzmann collision operator, $Q(f,f)$, whose Fourier transform is given by a weighted convolution. The truncated collision operator models the situation in which two colliding particles ignore each other if their relative speed exceeds a threshold, $g_{\rm tr}$. We demonstrate that the choice of truncation parameter plays a critical role in the accuracy of the numerical computation of Q. Significantly, if $g_{\rm tr}$ is too large, then accurate numerical computation of the weighted convolution integral is not feasible, since the decay rate and degree of oscillation of the convolution weighting function both increase as $g_{\rm tr}$ increases. We derive an upper bound on the pointwise error between Q and $Q^{\rm tr}$, assuming that both operators are computed exactly. This bound provides some additional theoretical justification for the spectral-Lagrangian method, and can be used to guide the choice of $g_{\rm tr}$ in numerical computations. We then demonstrate how to choose $g_{\rm tr}$ and the numerical discretization parameters so that the computation of the truncated collision operator is a good approximation to Q in the low probability tails. Finally, for several different initial conditions, we demonstrate the feasibility of accurately computing the time evolution of the velocity pdf down to probability density levels ranging from 10^{-5} to 10^{-9}.

Keywords: Boltzmann collision operator, spectral numerical method, low-probability tails

*Corresponding author

Email addresses: zweck@utdallas.edu (John Zweck), yanpingchen123@yahoo.com (Yanping Chen), goeckner@utdallas.edu (Matthew J. Goeckner), yshen@ku.edu (Yannan Shen)

2020 MSC: 35Q20, 35R09, 82C40, 82D10, 65Z05

1. Introduction

The motivation for this work is to develop improved computational tools for the simulation of low-probability, high-energy processes in non-equilibrium, low-temperature plasmas. Our interest is in kinetic models for the evolution of the velocity probability density function (pdf) of each particle species in a plasma. Such models are based on the Boltzmann equation which governs both the transport of, and collisions between, particles. In plasma systems, gas-phase chemistry and surface kinetics are largely driven by collision processes between high-energy electrons in the plasma and molecules in the gas phase [1]. Reaction rates in the gas phase are determined by the overlap between the electron velocity pdf and the electron-impact cross sections of the various species. Accurate calculation of the low-probability tails of the electron velocity pdf is therefore critical. If the plasma is in thermal equilibrium, the electron velocity pdf can often be assumed to be Maxwellian. However, experimental results demonstrate that the Maxwellian assumption is often invalid [2, 3, 4, 5, 6], especially for pulsed plasmas where the velocity pdf may depend strongly on both spatial position and on time [7].

The Direct Simulation Monte Carlo method (DSMC) is often used to numerically model collision processes in inhomogeneous (position-dependent) systems, and in systems that are not in thermal equilibrium. This method was initially developed by Bird [8] and Nanbu [9]. Wagner proved that solutions obtained using the DSMC method converge to the solution of the Boltzmann equation [10]. More recently, Rjasanow, Gamba, and Wagner modified the DSMC method to compute the low-probability tails of steady state solutions [11, 12]. Although they have proved effective in many situations, the statistical uncertainties in these methods can be challenging to resolve for systems that are not in thermal equilibrium [13].

Rather than attempting to model a realistic plasma system, in this paper we focus on the narrower goal of computing the velocity pdf, f, of a particle species (such as the electrons) down into the low-probability tails under the assumption that $f = f(t, \boldsymbol{v})$ satisfies an initial-value problem for the homogeneous Boltzmann equation,

$$\frac{\partial f}{\partial t} \;=\; Q(f, f). \tag{1}$$

Here, the Boltzmann collision operator, Q, is a bilinear integral operator that is defined in terms of a kernel that models a binary collision process. Although it omits much of the physics, this computation is nevertheless challenging because for each time, t, and each point in a 3-dimensional space of velocities, $\boldsymbol{v}$, the evaluation of $Q(f,f)(t,\boldsymbol{v})$ involves the computation of a 5-dimensional integral over a space of velocities and angular directions, resulting in a computational cost of order $\mathcal{O}(N^8)$.

Over the last two decades there have been several major advances that have enabled more efficient computation of the Boltzmann collision operator. An important class of deterministic methods are the spectral methods which include the Fourier-Galerkin methods of Pareschi and his collaborators [14, 15, 16], the spectral-Lagrangian methods of Gamba and her group [17, 18, 13, 19, 20, 21], and the more recent Petrov-Galerkin method of Gamba and Rjasanow [22].

With the Fourier-Galerkin method of Pareschi and Russo [16], the velocity pdf is assumed to be compactly supported and is approximated by a finite Fourier series. The Boltzmann collision operator then takes the form of a weighted discrete convolution operator where the weights are given in terms of the collision kernel. The resulting numerical scheme has a computational cost of $\mathcal{O}(N^6)$, where N is the number of discretization points in each velocity dimension, which represents a substantial improvement over the $\mathcal{O}(N^8)$ cost of direct numerical integration of the collision operator. Moreover, the method is spectrally accurate and conserves mass. However, due to the use of a Fourier series representation, positivity of the solution is not guaranteed, and non-physical high energy collisions are incorporated into the model due to the periodization and truncation of the velocity pdf and the collision operator. Building on this approach, Gamba et al. [18] developed a $\mathcal{O}(MN^4 \log N)$ algorithm with $M \ll N^2$, valid for arbitrary collision kernels, in which a pure convolution structure is achieved by numerical quadrature of the integral defining the convolution weighting function. Other advances along these lines include a method of Fonn et al. [23] that operates on a sparse set of Fourier modes, and a method of Cai et al. [24] that preserves positivity at Fourier collocation points and satisfies the H-theorem.

Compared to the Fourier-Galerkin methods, the spectral-Lagrangian method of Gamba and Tharkabhushanam [13] has the advantage that it provides a general framework for arbitrary collision kernels with either elastic or inelastic binary interactions, does not require periodization of f, and enforces conservation of moments through solution of an auxiliary constrained optimization

problem. The method is based on a formula for the Fourier transform of the collision operator in the form of a weighted convolution,

$$\widehat{Q}(f,f)(\boldsymbol{\zeta}) = (2\pi)^{-3/2} \int_{\mathbb{R}^3} \widehat{f}(\boldsymbol{\zeta}-\boldsymbol{\xi})\widehat{f}(\boldsymbol{\xi})\widehat{G}(\boldsymbol{\xi},\boldsymbol{\zeta})\, d\boldsymbol{\xi}, \tag{2}$$

where $\widehat{G}$ is a convolution weighting function that can be precomputed. The computational cost of the method is therefore the cost of numerically computing the integrals (2) for all $\boldsymbol{\zeta} \in \mathbb{R}^3$, which is $\mathcal{O}(N^6)$. Analogous to [18], Gamba et al. [25] obtained an approximate formula for $\widehat{G}$ which enables (2) to be expressed as a pure convolution that can be sped up using the fast Fourier transform to yield a $\mathcal{O}(MN^4 \log N)$ algorithm with $M \ll N^2$.

Alonso, Gamba, and Tharkabhushanam [26] analyzed the accuracy and consistency of the spectral-Lagrangian method. They restricted f and $Q(f,f)$ to a finite rectangular domain, $\Omega_L \subset \mathbb{R}^3$, of side-length, L, in velocity space and then orthogonally projected onto an N-dimensional Fourier series basis yielding the initial value problem,

$$\frac{\partial h}{\partial t} \;=\; \Pi^N Q(h,h), \qquad \text{in } (0,T] \times \Omega_L, \tag{3}$$

with $h(0,\boldsymbol{v}) = \Pi^N f(0,\boldsymbol{v})$. (Here Π^N is the projection operator.) To enforce conservation of mass, momentum, and energy (for elastic collisions), they used the method of Lagrange multipliers to replace the the right-hand side of (3) by the $L^2(\Omega_L)$-closest function to $\Pi^N Q(h,h)$ with zero mass, momentum, and energy. They then proved that for a large class of initial data, one can choose the size of the truncated domain, Ω_L, the number of Fourier modes, N, and the final simulation time, T, so that the solution, h, agrees with the equilibrium Maxwellian distribution to within a desired tolerance in a suitable Sobolev norm.

The convolution weighting function, $\widehat{G}(\boldsymbol{\xi},\boldsymbol{\zeta})$, in (2) is given as the Fourier transform with respect to $\boldsymbol{g}$ of a kernel, $G(\boldsymbol{\xi},\boldsymbol{g})$. To avoid the introduction of a divergent improper integral, the integral defining this Fourier transform must be taken over a finite ball, $|\boldsymbol{g}| \le g_{\text{tr}}$, rather than over all of $\mathbb{R}^3$. Therefore, the spectral-Lagrangian method is based on an approximation, Q^{tr}, of Q, which we refer to as the truncated collision operator. In their proof of an existence and uniqueness theorem for solutions of (1), Cercignani et al. [27] show that Q^{tr} converges weakly to Q as $g_{\text{tr}} \to \infty$. Physically, Q^{tr} models the situation in which two colliding particles ignore each other if their relative

speed exceeds the threshold, $g_{\rm tr}$ [27]. Pareschi and Russo [16], showed that if the velocity pdf has compact support in a ball of radius R then $Q = Q^{\rm tr}$ provided that $g_{\rm tr} \geq 2R$. They used this observation to avoid aliasing in their method to compute Q using a Fourier series approximation of f.[1] In a similar vein, Gamba and Tharkabhushanam showed that if the velocity pdf has compact support in the box, Ω_L, then $Q = Q^{\rm tr}$ provided that $g_{\rm tr} \geq 2\sqrt{3}L$. However, in their analysis of the method, Alonso et al. [26] assume that the function, $Q^{\rm tr}(f, f)$, is computed exactly from f, that is, they do not analyze the error in the numerical computation of the integral (2) for the Fourier transform of the truncated collision operator.

The first goal of this paper is to demonstrate that with the method of Gamba and Tharkabhushanam, the choice of the truncation parameter, $g_{\rm tr}$, plays a critical role in the accuracy of the numerical computation of Q. Clearly, if $g_{\rm tr}$ is too small then $Q^{\rm tr}$ will not be a good approximation to Q. However, if $g_{\rm tr}$ is too large then accurate numerical computation of the convolution integral (2) is not possible since the convolution weighting function, $\widehat{G}$, is a slowly decaying oscillatory function of $\boldsymbol{\xi}$ whose degree of oscillation increases as $g_{\rm tr}$ increases. Indeed, with Gamba and Tharkabhushanam's theoretical choice of $g_{\rm tr} = 2\sqrt{3}L$, we show that the numerically computed collision operator is a poor approximation. In unpublished work, Haack [28] instead uses $g_{\rm tr} = L$. However he provides no explanation for the smaller choice of $g_{\rm tr}$.

Our second goal is to derive an upper bound on the pointwise error between Q and $Q^{\rm tr}$, assuming that both operators are computed exactly. This error estimate can be viewed as a generalization to velocity pdfs without compact support of the formula for $g_{\rm tr}$ obtained by Gamba and Tharkabhushanam. In particular our estimate yields the following *simple strategy* for choosing the parameter, $g_{\rm tr}$, in numerical computations of the low-probability tails. Specifically, to guarantee that $Q^{\rm tr}$ is an accurate approximation to Q at $\mathbf{v}$, we should choose $g_{\rm tr}$ to be slightly larger than $|\mathbf{v}|$, *irrespective of the probability level at* $\mathbf{v}$. In particular, our error bound provides a theoretical justification for Haack's choice of $g_{\rm tr} = L$. We obtained this error bound without regard to any truncation or discretization of the domain of the ve-

[1] We note that the Fourier series method of Pareschi and Russo has a different character to the spectral-Lagrangian method of Gamba and Tharkabhushanam, which does not have to avoid the possibility of aliasing effects.

locity pdf or the collision operator. In particular, our bound has nothing to do with the need to avoid aliasing in the Fourier series approximations of f in methods such as that of Pareschi and Russo. Indeed, we emphasize that the method of Gamba and Tharkabhushanam that we are analyzing here is based on a formula for Q in terms of a continuous Fourier transform and so does not require any periodization of the domain of f [13].

Our third goal is to perform a series of simulation studies that demonstrate how to choose $g_{\rm tr}$ and the numerical discretization parameters so that the numerical computation of the truncated collision operator is a good approximation to Q in the low probability tails. In particular, we demonstrate that when we use the simple strategy described above to select $g_{\rm tr}$ to guarantee that $Q^{\rm tr}$ is close to Q at $\mathbf{v}$, then it is often feasible to numerically compute the generalized convolution integral for $Q^{\rm tr}$ with sufficient accuracy at $\mathbf{v}$. Finally, for several different initial conditions, we use the selected values of $g_{\rm tr}$ to show that the time evolution of the velocity pdf can be computed accurately down to probability density levels ranging from 10^{-5} to 10^{-9}.

In Section 2, we review the spectral-Lagrangian method of Gamba and Tharkabhushanam, and in Section 3 we present the results of preliminary numerical simulations that demonstrate that the choice $g_{\rm tr}$ plays a critical role in the accuracy of the numerical computation of Q. In Section 4, we derive the bound on the relative error between $Q^{\rm tr}$ and Q. In Section 5, we discuss some implementation details, and in Section 6 we present the results of our numerical simulations. Finally, in Section 7 we make some conclusions.

2. The spectral-Lagrangian method for the Boltzmann equation

In this section, we review the spectral-Lagrangian method for the homogeneous Boltzmann equation developed by Gamba and Tharkabhushanam [13]. This method reduces the computational cost of the collision operator from $\mathcal{O}(N^8)$ to $\mathcal{O}(N^6)$, where N is the number of discretization points in each velocity dimension.

The homogeneous Boltzmann equation for the velocity probability density function (pdf), $f = f(t, \boldsymbol{v})$, of particles of species due to elastic collisions with particles of the same species is given by

$$\frac{\partial f}{\partial t} \;=\; Q(f, f), \tag{4}$$

where the Boltzmann collision operator, $Q := Q(f, f)$, is given by

$$Q(\boldsymbol{v}) = \int_{\mathbb{R}^3} \int_{S^2} \left[f(\boldsymbol{v}') f(\boldsymbol{w}') - f(\boldsymbol{v}) f(\boldsymbol{v} + \boldsymbol{g}) \right] B \left(g, \frac{\boldsymbol{g} \cdot \Theta}{g} \right) d\Theta d\boldsymbol{g}. \tag{5}$$

Here $\boldsymbol{g} = \boldsymbol{w} - \boldsymbol{v}$ is the relative pre-collisional velocity and $g = |\boldsymbol{g}|$ is the relative speed. Assuming that the particles have unit mass, the post-collisional velocities, $\boldsymbol{v}'$ and $\boldsymbol{w}'$, are given in terms of the pre-collisional velocities, $\boldsymbol{v}$ and $\boldsymbol{w}$, by

$$\boldsymbol{v}' = \boldsymbol{v} + \tfrac{1}{2} \left(\boldsymbol{g} - g \, \Theta \right), \qquad \boldsymbol{w}' = \boldsymbol{w} - \tfrac{1}{2} \left(\boldsymbol{g} - g \, \Theta \right), \tag{6}$$

for some direction vector, Θ, on the unit sphere, S^2. We assume that the collisions are modeled using an interparticle potential of the form, $\phi(r) = r^{-(s-1)}$, for some $1 < s \leq \infty$. In this case, the collision kernel, B, is of the form $B(g, \chi) = g^{\lambda} \widetilde{B}(\cos \chi)$, where $\lambda = (s-5)/(s-1)$, and the scattering angle, χ, is given by $\cos \chi = (\boldsymbol{g} \cdot \Theta)/g$. For the main results in this paper, we further assume that $0 \leq \lambda \leq 1$, and that the collisions are isotropic, so that $\widetilde{B}$ is constant. The cases $\lambda = 0$ and $\lambda = 1$ are those of Maxwell and hard-sphere collisions, respectively.

Rather than computing Q itself, Gamba and Tharkabhushanam consider a truncation, Q^{tr}, of the collision operator defined by

$$Q^{\mathrm{tr}}(\boldsymbol{v}) = \int_{|\boldsymbol{g}| \leq g_{\mathrm{tr}}} \int_{S^2} \left[f(\boldsymbol{v}') f(\boldsymbol{w}') - f(\boldsymbol{v}) f(\boldsymbol{v} + \boldsymbol{g}) \right] B \left(g, \frac{\boldsymbol{g} \cdot \Theta}{g} \right) d\Theta d\boldsymbol{g}, \tag{7}$$

for some choice of truncation parameter, g_{tr}. To explain why it is necessary to truncate the $\boldsymbol{g}$-integral in (7), we briefly review the derivation of the method.

We define the Fourier transform of a function, F, on velocity space to be

$$\widehat{F}(\boldsymbol{\zeta}) := (2\pi)^{-3/2} \int_{\mathbb{R}^3} F(\boldsymbol{v}) e^{-i \boldsymbol{\zeta} \cdot \boldsymbol{v}} d\boldsymbol{v}. \tag{8}$$

Using the weak form of the collision operator, Gamba and Tharkabhushanam first show that

$$\widehat{Q}^{\mathrm{tr}}(\boldsymbol{\zeta}) = (2\pi)^{-3/2} \int_{|\boldsymbol{g}| \leq g_{\mathrm{tr}}} G(\boldsymbol{g}, \boldsymbol{\zeta}) \int_{\mathbb{R}^3} f(\boldsymbol{v}) f(\boldsymbol{v} - \boldsymbol{g}) \, e^{-i \boldsymbol{\zeta} \cdot \boldsymbol{v}} \, d\boldsymbol{v} d\boldsymbol{g}, \tag{9}$$

where

$$G(\boldsymbol{g},\boldsymbol{\zeta}) = e^{\frac{i}{2}\boldsymbol{\zeta}\cdot\boldsymbol{g}} \int_{S^2} B\left(g, \frac{\boldsymbol{g}\cdot\Theta}{g}\right) e^{-\frac{i}{2}g\,\boldsymbol{\zeta}\cdot\Theta} d\Theta \;-\; \int_{S^2} B\left(g, \frac{\boldsymbol{g}\cdot\Theta}{g}\right) d\Theta. \quad (10)$$

In the special case of isotropic, inter-particle collisions, the kernel, G, is given by

$$G(\boldsymbol{g},\boldsymbol{\zeta}) = 4\pi\widetilde{B} g^{\lambda} \left[e^{\frac{i}{2}\boldsymbol{\zeta}\cdot\boldsymbol{g}}\ \mathrm{sinc}\,(g\zeta/2) - 1\right], \quad (11)$$

where $\zeta = |\boldsymbol{\zeta}|$.

Although G is not an integrable function of $\boldsymbol{g}$ on $\mathbb{R}^3$, it does define a tempered distribution [29]. Therefore, when $g_{\mathrm{tr}} = \infty$, the integral (9) for $\widehat{Q}$ converges since the velocity pdfs decay exponentially. However, the final step in the derivation of the method involves taking the Fourier transform of G with respect to $\boldsymbol{g}$, which is a divergent improper integral over $\mathbb{R}^3$ when $g_{\mathrm{tr}} = \infty$. This is why it is necessary to truncate the $\mathbf{g}$-integral in (7). Specifically, we define the convolution weighting function by

$$\widehat{G}^{\mathrm{tr}}(\boldsymbol{\xi},\boldsymbol{\zeta}) = \int_{|\boldsymbol{g}|\le g_{\mathrm{tr}}} G(\boldsymbol{g},\boldsymbol{\zeta}) e^{-i\,\boldsymbol{\xi}\cdot\boldsymbol{g}}\, d\boldsymbol{g}. \quad (12)$$

Then, by the convolution theorem, the Fourier transform of the truncated collision operator is given by a generalized convolution integral of the form

$$\widehat{Q}^{\mathrm{tr}}(\boldsymbol{\zeta}) = (2\pi)^{-3/2} \int_{\mathbb{R}^3} \widehat{f}(\boldsymbol{\zeta}-\boldsymbol{\xi})\widehat{f}(\boldsymbol{\xi})\widehat{G}^{\mathrm{tr}}(\boldsymbol{\xi},\boldsymbol{\zeta})\, d\boldsymbol{\xi}. \quad (13)$$

Since the convolution weighting function is independent of the velocity pdfs, $\widehat{G}^{\mathrm{tr}}$ can be precomputed. Therefore the computational cost of computing the collision operator using (13) is $\mathcal{O}(N^6)$.

Haack et al. [28] showed that in the special case of isotropic Maxwell collisions, for which $B = (4\pi)^{-1}$, we have

$$\widehat{G}^{\mathrm{tr}}(\boldsymbol{\xi},\boldsymbol{\zeta}) \;=\; \widehat{G}_1(\zeta/2, |\boldsymbol{\xi}-\boldsymbol{\zeta}/2|) - \widehat{G}_2(\xi), \quad (14)$$

with

$$\widehat{G}_1(X,Y) = \frac{2\pi}{pqXY}\left[q\,\sin(g_{\mathrm{tr}}\,p) - p\,\sin(g_{\mathrm{tr}}\,q)\right], \quad (15)$$

$$\widehat{G}_2(Z) = \frac{4\pi}{Z^3}\left[\sin(g_{\mathrm{tr}}Z) - g_{\mathrm{tr}}\,Z\cos(g_{\mathrm{tr}}Z)\right], \quad (16)$$

where $p = X - Y$ and $q = X + Y$.

3. Preliminary numerical study

In this section, we demonstrate that the choice of the truncation parameter, $g_{\rm tr}$, in (7) plays a critical role in the accuracy of the numerical computation of Q. Clearly, if $g_{\rm tr}$ is too small then $Q^{\rm tr}$ will not be a good approximation to Q. On the other hand, if $g_{\rm tr}$ is too large then accurate numerical computation of the convolution integral (13) is not possible since the convolution weighting function, $\widehat{G}^{\rm tr}$, in (14) is a slowly decaying oscillatory function of $\boldsymbol{\xi}$ whose degree of oscillation increases as $g_{\rm tr}$ increases.

Gamba and Tharkabhushanam show that if the velocity pdfs are compactly supported, then there is a value $g_{\rm tr} < \infty$ so that $Q = Q^{\rm tr}$. Specifically, they show that if the velocity pdfs are zero outside a box $[-L, L]^3 \subset \mathbb{R}^3$, then $f(\boldsymbol{v})f(\boldsymbol{w}-\boldsymbol{g}) = 0$ whenever $\boldsymbol{v} \in [-L, L]^3$ and $|\boldsymbol{g}| > g_{\rm max}$, where $g_{\rm max} = 2\sqrt{3}L$. Therefore, if we choose $g_{\rm tr} = g_{\rm max}$, then $Q = Q^{\rm tr}$, by (9). In an unpublished article, Haack [28] instead uses $g_{\rm tr} = L$. However he provides no explanation for the smaller choice of $g_{\rm tr}$. As we now show, the choice of $g_{\rm tr}$ plays a critical role in the accuracy of the numerical computation. To do so, we compute the collision operator for the spherically symmetric, analytical solution of (4) derived by Bobylev, Krook and Wu [30, 31], which is given by

$$f_{\rm BKW}(\boldsymbol{v}, t) = \frac{e^{-v^2/(2KT)}}{2(2\pi KT)^{3/2}} \left(\frac{5K-3}{K} + \frac{1-K}{K^2} \frac{v^2}{T} \right), \tag{17}$$

where $v = |\boldsymbol{v}|$ and $K = 1 - e^{-t/6}$. The parameter, T, is the temperature, which we set to $T = 1$. We compute the collision operator at the initial time of $t_0 = 5.5$, which is chosen to ensure that $f_{\rm BKW} > 0$. Following Haack [28], we choose the half-width of the computational domain to be $L = 2R$, where R is a measure of the effective support for the velocity pdf. Based on a suggestion of Bobylev and Rjasnow [32], Haack chooses $R = 2\sqrt{2T}$, where T is the temperature of the distribution, which results in $L \approx 5.66$. This choice is justified by the observation that the velocity pdf typically decreases as does $\exp(-v^2/2T)$ for large v.

In Fig. 1 (left) we plot slices of the collision operator on a linear scale with $g_{\rm tr} = L$ and $g_{\rm tr} = 2\sqrt{3}L$. For these results we used $N = 48$ discretization points in each velocity direction. The result with $g_{\rm tr} = L$ agrees well with the analytical formula for Q obtained using (4) and (17). However, the result with $g_{\rm tr} = 2\sqrt{3}L$ is far from being correct, which suggests that in their numerical simulations Gamba and Tharkabhushanam actually used a

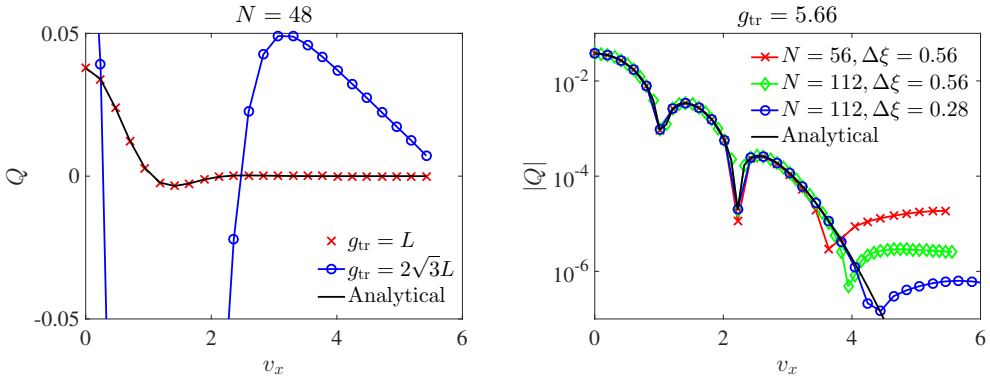

Figure 1: Slices in the v_x-direction of the collision operator at $(v_y, v_z) = (0, 0)$ for the BKW pdf (17) with $T = 1$ at $t = 5.5$. Left: Linear scale plots of Q for the values of $g_{\rm tr}$ obtained using the formulae given in [13] and [28] with $N = 48$ discretization points in each velocity direction. Right: Log scale plots of $|Q|$ for the value of $g_{\rm tr}$ given in [28] for different values of N and $\Delta\xi$. In both panels, the black solid curves show the results obtained using the analytical formula (17).

significantly smaller value of $g_{\rm tr}$, although they do not state which value they chose.

The reason for the lack of agreement with $g_{\rm tr} = 2\sqrt{3}L$ is that the integral (13) for $\widehat{Q}^{\rm tr}$ is numerically computed using values of $\widehat{f}$ and $\widehat{G}^{\rm tr}$ on a grid with spacing

$$\Delta\xi = \frac{\pi}{L} = \frac{2\sqrt{3}\pi}{g_{\rm tr}}. \tag{18}$$

This grid spacing is determined by the standard discretization of the Fourier transform. With this grid spacing there can be significant error in the numerical computation of the integral, since as we see from (15) and (16), the kernel, $\widehat{G}^{\rm tr}$, oscillates on a length scale of approximately $2\pi/g_{\rm tr}$. Increasing the number of discretization points, N, in each velocity dimension does not change $\Delta\xi$. On the other hand, the agreement is much better with $g_{\rm tr} = L$, since the frequency of oscillation of $\widehat{G}^{\rm tr}$ is approximately half that of the sampling frequency, $\Delta\xi = \pi/g_{\rm tr}$, in accord with the Nyquist-Shannon sampling theorem.

Because we are interested in computing the low-probabilty tails of the velocity pdf, it is important to determine how the choice of $g_{\rm tr}$ affects the relative error in the numerically computed values of collision operator at large speeds, $v = |\mathbf{v}|$. To start investigating this question, in Fig. 1 (right) we plot

slices of the absolute value of the collision operator on a logarithmic scale. We note that the cusps evident in the log-scale plots occur where Q changes sign. The three numerical results were obtained using $g_{\rm tr} = 5.66$ but with different choices for N and for the grid spacing $\Delta\xi = \pi/L$ used in the numerical computation of the integral (13). The red line with crosses and the green line with diamonds shows the results with $N = 56$ and $N = 112$, respectively. In both cases we choose $L = g_{\rm tr} = 5.66$, which results in $\Delta\xi = 0.56$. We see from these results that doubling N increases the accuracy of the computation by about an order of magnitude. The reason is that $\widehat{G}^{\rm tr}$ decays slowly as $|\boldsymbol{\xi}| \to \infty$ and increasing N increases the size of the domain of integration in frequency space. The blue curve with circles shows the result with $N = 112$ and $L = 2g_{\rm tr} = 11.32$, so that $\Delta\xi = 0.28$. Comparing the red and blue curves, we see that halving $\Delta\xi$ increases the accuracy of the computation by about two orders of magnitude. The reason is the smaller grid spacing better captures the oscillations of $\widehat{G}^{\rm tr}$.

One of our main goals in this paper is to fix L and investigate how small we can choose both $g_{\rm tr}$ and N so as to accurately compute the velocity pdf down to a desired probability level. If we let $Q^{\rm NC}$ denote the collision operator obtained by numerically computating of $Q^{\rm tr}$, then the total error,

$$\mathcal{E}_{\rm tot} \;:=\; \left|Q - Q^{\rm NC}\right|, \tag{19}$$

is bounded by

$$\mathcal{E}_{\rm tot} \;\le\; \left|Q - Q^{\rm tr}\right| \;+\; \left|Q^{\rm tr} - Q^{\rm NC}\right|. \tag{20}$$

The first term on the right hand side of (20) is the error inherent in the truncation of the collision operator, and the second term is the error in the numerical computation of the truncated operator. Since in practice, we have limited computational resources the choice of $g_{\rm tr}$ involves a trade off between these two sources of error.

4. An error estimate for the truncated collision operator

In this section, we first review a theorem of Cercignani et al. [27] on the convergence of $Q^{\rm tr}$ to Q as $g_{\rm tr} \to \infty$. However, since this theorem does not include an error bound, it is of limited utility for numerical computation. Then, we derive an upper bound on the pointwise error between Q and $Q^{\rm tr}$, assuming that both operators are computed exactly. This bound provides some additional theoretical justification for the spectral-Lagrangian method.

In Section 6, we will use this upper bound to guide the choice of $g_{\rm tr}$ in numerical computations.

Cercignani et al. [27] use the truncated collision operator in a proof of an existence and uniqueness theorem for solutions of the homogeneous Boltzmann equation. In their proof they consider the initial value problem,

$$\begin{aligned} \frac{\partial f^M}{\partial t} &= Q^M(f^M, f^M), \\ f^M(0,\cdot) &= f_0, \end{aligned} \tag{21}$$

where $Q^M = Q^{\rm tr}$ with $g_{\rm tr} = M < \infty$. They show that (21) has a unique nonnegative solution $f^M \in C^1([0,T], L^1(\mathbb{R}^3))$ for all $T > 0$, provided that $f_0 \in L^1(\mathbb{R}^3)$ is nonnegative. In addition, they show that the total mass, momentum, and energy are conserved by (21). Applying the Dunford-Pettis theorem to the set $\{f^M\}$ in $C^1([0,T], L^1(\mathbb{R}^3))$, they extract a weakly convergent subsequence $f^n \rightharpoonup f$, with $f \in C^1([0,T], L^1(\mathbb{R}^3))$ nonnegative, and prove that $Q^{M_n}(f^n, f^n) \rightharpoonup Q(f,f)$. Here, by weak convergence we mean convergence of the sequence obtained after integration against a test function in $L^\infty(\mathbb{R}^3)$.

To assess the trade off discussed at the end of Section 3, we now present an upper bound for the error inherent in the truncation of Q, *i.e.*, for the first term on the right hand side of (20). Specifically, we let

$$\mathcal{E}_{\rm tr}(\mathbf{v}) := \left| Q(\mathbf{v}) - Q^{\rm tr}(\mathbf{v}) \right|, \tag{22}$$

where $Q = Q(f,f)$ and $Q^{\rm tr} = Q^{\rm tr}(f,f)$. Since these two collision operators are defined in terms of the same velocity pdf, f, this result has a different character than that of Cercignani.

To obtain this result, rather than assuming that the support of f is compact, we instead assume that f is bounded above by a Maxwellian pdf. For Maxwell-type collisions between particles of the same type, Bobylev and Gamba [33] proved that, if the initial condition satisfies $f_0(\boldsymbol{v}) \le c_0\, e^{-k_0 v^2}$, then there are constants $c \ge c_0$ and $k \le k_0$ so that $f(\boldsymbol{v},t) \le c\, e^{-kv^2}$ for all $t > 0$. Moreover, they provide formulae for c and k in terms of c_0, k_0, and the initial pdf f_0. Gamba et al. [34] proved similar results for other interparticle collision kernels. Consequently, the assumptions we make in the following theorem and in its corollary are reasonable.

Theorem 1. *Suppose that $f(\boldsymbol{v}) \le c\, e^{-kv^2}$, where $v = |\boldsymbol{v}|$, and that the collision kernel is of the form $B(g,\chi) = g^\lambda\, \widetilde{B}$, where $\widetilde{B}$ is a positive constant*

and $0 \le \lambda \le 1$. *Then, the error* (22) *in the truncation of the collision operator is bounded by*

$$\mathcal{E}_{\rm tr}(\mathbf{v}) \;\le\; \mathcal{E}_{\rm tr}^{\rm UB}(g_{tr}, v) := c\exp(-kv^2)\,\mathcal{E}_{\rm rel}(g_{\rm tr}, v), \tag{23}$$

where

$$\mathcal{E}_{\rm rel}(g_{\rm tr}, v) \;:=\; 16\pi^2 \widetilde{B}\, c \int_{g=g_{\rm tr}}^{\infty} e^{-k(v-g)^2} \left[\frac{1-e^{-4kvg}}{4kvg}\right] g^{\lambda+2}\, dg. \tag{24}$$

Since Q is the rate of change of f, we expect $Q(\mathbf{v})$ to be on the order of $c\exp(-kv^2)$ or less. Therefore, we can regard the error, $\mathcal{E}_{\rm rel}$, in (24) as a measure of the relative error between Q and $Q^{\rm tr}$. Note that since Q has zeros, we have defined this error to be relative to a Maxwellian pdf rather than to Q. The upper bound, $\mathcal{E}_{\rm rel}$, in (24) can be used to guide the choice of $g_{\rm tr}$ in numerical simulations by ensuring that $\mathcal{E}_{\rm rel}(g_{\rm tr}, v) < 10^{-m}$ for a desired value of m, over a given range of values for v.

Proof. Using the assumptions in the statement of the theorem,

$$|Q(\boldsymbol{v}) - Q^{\rm tr}(\boldsymbol{v})| \;\le\; \widetilde{B}\max\left\{\mathcal{E}_1, \mathcal{E}_2\right\}, \tag{25}$$

where

$$\mathcal{E}_1 = \int\limits_{|\mathbf{g}|\ge g_{\rm tr}} \int_{S^2} f\left(\boldsymbol{v} + \tfrac{1}{2}\,(\boldsymbol{g} - g\,\Theta)\right) f\left(\boldsymbol{v} + \tfrac{1}{2}\,(\boldsymbol{g} + g\,\Theta)\right) g^{\lambda}\, d\Theta\, d\boldsymbol{g}, \tag{26}$$

and

$$\mathcal{E}_2 = \int\limits_{|\boldsymbol{g}|\ge g_{\rm tr}} \int_{S^2} f(\boldsymbol{v}) f(\boldsymbol{v}+\boldsymbol{g})\, g^{\lambda}\, d\Theta\, d\boldsymbol{g}. \tag{27}$$

The inequality (25) holds since $\mathcal{E}_1$ and $\mathcal{E}_2$ are both positive. Using the upper bound we have assumed for f, we find that

$$\begin{aligned}
\mathcal{E}_2 \;&\le\; 4\pi c^2 e^{-2kv^2} \int\limits_{|\boldsymbol{g}|\ge g_{\rm tr}} e^{-k(2\boldsymbol{v}\cdot\boldsymbol{g}+g^2)}\, g^{\lambda}\, d\boldsymbol{g} && (28)\\
&=\; 8\pi^2 c^2 e^{-2kv^2} \int_{g_{\rm tr}}^{\infty} e^{-kg^2} g^{\lambda+2} \int_0^{\pi} e^{-2\,kvg\cos\phi}\, \sin\phi\, d\phi\, dg\\
&=\; 16\pi^2\, c^2\, e^{-kv^2} \int_{g_{\rm tr}}^{\infty} e^{-k(v-g)^2} \left[\frac{1-e^{-4kvg}}{4kvg}\right] g^{\lambda+2}\, dg. && (29)
\end{aligned}$$

Similarly,

$$\mathcal{E}_1 \;\le\; c^2 \int\limits_{|\boldsymbol{g}|\ge g_{\rm tr}} \int_{S^2} e^{-k|\boldsymbol{v}+\frac{1}{2}(\boldsymbol{g}-g\Theta)|^2}\, e^{-k|\boldsymbol{v}+\frac{1}{2}(\boldsymbol{g}+g\Theta)|^2}\, g^\lambda d\Theta\, d\boldsymbol{g} \tag{30}$$

$$\le\; 4\pi c^2\, e^{-2kv^2} \int\limits_{|\boldsymbol{g}|\ge g_{\rm tr}} e^{-k(2\boldsymbol{v}\cdot\boldsymbol{g}+g^2)} g^\lambda\, d\boldsymbol{g}. \tag{31}$$

As in (28) and (29), we find that

$$\mathcal{E}_1 \le 16\pi^2\, c^2\, e^{-kv^2} \int_{g_{\rm tr}}^\infty e^{-k(v-g)^2} \left[\frac{1-e^{-4kvg}}{4kvg}\right] g^{\lambda+2}\, dg. \tag{32}$$

The required estimate now follows from (25), (32), and the fact that the right hand side of (29) is bounded above by the right hand side of (32). □

Corollary 1. *Suppose that the assumptions of Theorem 1 hold and that $\lambda = 0$. Then, provided k and $g_{\rm tr}$ are both large enough, we have the asymptotic formulae*

$$\mathcal{E}_{\rm rel}(g_{\rm tr}, v) \;\approx\; \begin{cases} c(\frac{\pi}{k})^{3/2} & \text{if } g_{\rm tr} < v, \\ \frac{1}{2}[c(\frac{\pi}{k})^{3/2} \;+\; \frac{1}{kg_{\rm tr}}] & \text{if } g_{\rm tr} = v, \\ \frac{\pi c}{2k^2}\, \frac{e^{-k(g_{\rm tr}-v)^2}}{g_{\rm tr}-v}\, \frac{g_{\rm tr}}{v} & \text{if } g_{\rm tr} > v. \end{cases} \tag{33}$$

In particular, if $g_{\rm tr} \gtrsim v \gg 0$, then

$$\mathcal{E}_{\rm rel}(g_{\rm tr}, v) \;\approx\; \frac{\pi c}{2k^2}\, \frac{e^{-k(g_{\rm tr}-v)^2}}{g_{\rm tr}-v}, \tag{34}$$

which is a rapidly decaying function of $g_{\rm tr} - v$.

Equation (34) yields the following simple strategy for choosing the parameter, $g_{\rm tr}$, in numerical computations of the low-probability tails. Specifically, to guarantee $Q^{\rm tr}$ is an accurate approximation to Q at $\mathbf{v}$, we should choose $g_{\rm tr}$ to be slightly larger than v. As we will see in Section 6, exactly how much larger depends on the values of c and k and the desired degree of accuracy.

Proof. Under the assumptions of (1),

$$\mathcal{E}(g_{\rm tr}, v) \;=\; 4\pi c \int_{g_{\rm tr}}^\infty e^{-k(v-g)^2}\, \frac{1-e^{-4kvg}}{4kvg}\, g^2\, dg. \tag{35}$$

In the cases that $g_{\rm tr} \le v$, we apply Laplace's method [35] as follows. First, recall that if a function $\phi : [a,b] \to \mathbb{R}$ has a single critical point at an interior point, $t_0 \in (a,b)$, which is the absolute minimum of ϕ, then for any sufficiently smooth function, f,

$$\int_a^b e^{-k\phi(t)}\, f(t)\, dt \;\approx\; \sqrt{\frac{2\pi}{k\phi''(t_0)}}\, e^{-k\phi(t_0)}\, f(t_0), \qquad \text{as } k \to \infty. \tag{36}$$

When $g_{\rm tr} < v$, the result follows by setting $t_0 = v$, and using the estimate $f(v) = \frac{c\pi}{k}(1 - e^{-4kv^2}) \approx \frac{c\pi}{k}$, provided $g_{\rm tr}$ is large enough. When $g_{\rm tr} = v$, the critical point, $t_0 = g_{\rm tr}$, of ϕ is an endpoint of the interval of integration. Then by [35, (5.1.17)], we find that

$$\mathcal{E}(g_{\rm tr}, g_{\rm tr}) \;\approx\; \frac{\pi c}{k g_{\rm tr}} \left[\sqrt{\frac{\pi}{4k}}\, g_{\rm tr}(1 - e^{-4kg_{\rm tr}^2}) + \tfrac{1}{2k}\left(1 - (1 + 4kg_{\rm tr}^2)e^{-4kg_{\rm tr}^2}\right)\right]. \tag{37}$$

The result now follows provided $g_{\rm tr}$ is large enough.

Finally, in the case $g_{\rm tr} > v$, the change of variables $t = (g-v)^2 - (g_{\rm tr}-v)^2$ transforms (35) to

$$\mathcal{E}(g_{\rm tr}, v) \;=\; 2\pi c\, e^{-k(g_{\rm tr}-v)^2} \int_0^\infty e^{-kt} F(\sqrt{t + (g_{\rm tr}-v)^2}\,;\, k, v)\, dt, \tag{38}$$

where

$$F(u\,;\, k, v) = \frac{1 - e^{-4kv(v+u)}}{4kvu}\; \frac{(v+u)^2}{u}. \tag{39}$$

The result now follows from Watson's Lemma [35], which states that in the limit as $k \to \infty$, we have that $\int_0^\infty e^{-kt} H(t)\, dt \approx H(0)/k$. Although (33) is only guaranteed to hold in the limit $k \to \infty$, in Section 6 we will show it that is quite accurate even for $k = \mathcal{O}(1)$. □

5. Numerical Method

We implement Gamba's method as in [13, 28]. The computational grids in velocity and Fourier space are defined in terms of a maximum speed, L, and the number of grid points, N, in each dimension. Unless otherwise noted, we use $L = 10$. We represent the velocity pdf on a domain $[-L, L]^3 \in \mathbb{R}^3$ using a regular grid, $v_k = -L + k\Delta v$, in each velocity dimension, where $\Delta v = 2L/N$. The corresponding domain in Fourier space is

$[-\zeta_{\max}, \zeta_{\max}]^3$, where $\zeta_{\max} = N\pi/2L$, with grid points, $\zeta_m = -\zeta_{\max} + m\Delta\zeta$, where $\Delta\zeta = \pi/L$. We calculate the integral (13) using the trapezoid rule, which—like the discrete Fourier transform—is spectrally accurate for functions that decay rapidly at the boundary of the computation domain [36]. In addition, for the numerical results in Sections 6.1–6.4 below we enforce conservation of the density, momentum, and energy using the Lagrangian projection method of [13], which amounts to projecting the collision operator onto a linear subspace in $L^2(\mathbb{R}^3)$. However, we found that the results in these subsections are visually indistinguishable from those we obtained without the application of the Lagrangian projection method. Because of the large cost of computing the collision operator, we use a multistep method to solve the system of differential equations corresponding to (4), which allows us to take larger time steps resulting in a fewer total number of function evaluations. Specifically, we used the fourth order Adams-Bashforth method [37]

$$f_{i+4} = f_{i+3} + \frac{\Delta t}{24}\Big[55Q_{i+3} - 59Q_{i+2} + 37Q_{i+1} - 9Q_i\Big], \tag{40}$$

where $f_i(\boldsymbol{v}) = f(t_i, \boldsymbol{v})$ and $Q_i = Q^{\mathrm{tr}}(f_i, f_i)$. To initialize this multistep method we used the fourth order Runge Kutta method to compute the solutions at the first four time steps.

6. Numerical Results

In this section we present the results of the numerical simulations we performed to test the limits of the spectral-Lagrangian method. We show results for the following choices of initial condition: a Maxwellian, the spherically symmetric, analytical solution of Bobylev, Krook and Wu [30, 31], a cylindrically symmetric modification of the BKW initial condition, and two mixtures of Maxwellians. We study the convergence of the numerically computed truncated collision operator, Q^{NC}, to the collision operator, Q, validate the bound we obtained for the relative error between Q^{tr} and Q, and compute the evolution of the velocity pdf to the equilibrium Maxwellian distribution. In these simulations our focus is on the accuracy with which the velocity pdfs can be computed in the low probability tails. Finally, we employ a simple model of a plasma to study the evolution of the velocity pdf of the electrons under the influence of an electron gun source, electron-electron collisions, and loss into a boundary sheath layer.

The simulations were performed on a 2.0 GHz Intel Xeon processor with 2 CPU's and 14 cores per CPU. The total simulation time (number of cores $\times$ time per core) for a single computation of the collision operator ranged from 24 seconds for $N = 24$ to 4.5 hours for $N = 72$, and scaled according to the theoretical $\mathcal{O}(N^6)$ cost.

6.1. The Maxwellian solution

If the initial velocity pdf is a Maxwellian, $f(\mathbf{v}) = (2\pi T)^{-3/2} \exp(-v^2/2T)$, then the collision operator is identically zero, $Q \equiv 0$. In Table 1, with $T = 1$, we plot the L^∞-error in the numerically computed truncation operator, Q^{NC}, for several pairs of values of N and $g_{\rm tr}$. When $g_{\rm tr} = 4$ and 8, the error decreases to the level of the round-off error for the Fourier transform as N increases from 24 to 72. However, when $g_{\rm tr} = 12$, the error does not converge to zero since the convolution weighting function, $\widehat{G}^{\rm tr}$, oscillates on a length scale that is close to $\Delta\xi = \Delta\zeta$. The results are significantly worse when $g_{\rm tr}$ is increased to 16 and 20. These results show that, if N is large enough to capture the slow decay of $\widehat{G}^{\rm tr}$ ($N \geq 48$), then we can obtain a large gain in the accuracy of the generalized convolution integral (13) for $\widehat{Q}^{\rm tr}$ by choosing $g_{\rm tr} < L$, thereby reducing the oscillation of $\widehat{G}^{\rm tr}$ relative to the grid spacing in Fourier space. For more general initial conditions, because $\widehat{f}$ is typically smoother than $\widehat{G}^{\rm tr}$, we expect a similar rate of convergence of $Q^{\rm tr}$ to $Q^{\rm NC}$, i.e., for the second term in (20). In the next subsections, for several choices of initial condition, we use the error bound in Theorem 1 to determine values of $g_{\rm tr}$ for which we can guarantee that the error in the second term in (20) is below a given threshold out to a given value of v.

	$g_{\rm tr} = 4$	$g_{\rm tr} = 8$	$g_{\rm tr} = 12$	$g_{\rm tr} = 16$	$g_{\rm tr} = 20$
$N = 24$	2×10^{-5}	3×10^{-5}	4×10^{-5}	2×10^{-4}	2×10^{-1}
$N = 36$	2×10^{-9}	4×10^{-9}	4×10^{-9}	2×10^{-4}	2×10^{-1}
$N = 48$	8×10^{-15}	1×10^{-14}	5×10^{-10}	2×10^{-4}	2×10^{-1}
$N = 72$	5×10^{-17}	5×10^{-17}	5×10^{-10}	2×10^{-4}	2×10^{-1}

Table 1: L^∞-error in Q^{NC} for the Maxwellian velocity pdf for different values of N and $g_{\rm tr}$.

6.2. The BKW solution

In this subsection, we compare the results obtained using the numerical method to the analytical solution, f_{BKW}, of Bobylev, Krook and Wu [30, 31] given in (17) with $T = 1$.

We begin by using Theorem 1 to select an appropriate value of the truncation parameter, g_{tr}, for the velocity pdf, f_{BKW}, at the initial time of $t = 5.5$. We consider two methods for selecting the Maxwellian upper bound required to apply the theorem. For Method I we choose the width parameter, k, in Theorem 1 to agree with the width of the Maxwellian pdf to which the initial condition converges as $t \to \infty$. This method gives $k = 3/2E$, where E is the (initial) energy. We then choose the parameter c to ensure that the resulting Maxwellian pdf is an upper bound for the velocity pdfs at the initial time. For the BKW pdf, Method I gives $k = 0.5$ and $c = 0.1$. For Method II, we use the tightest upper Maxwellian bound we could find for the initial velocity pdf, which resulted in $k = 0.8$ and $c = 1$.

In Fig. 2 (left), we plot the initial BKW pdf and the two Maxwellian bounds, and in Fig. 2 (middle) we show a contour plot of the bound, $\mathcal{E}_{\mathrm{rel}}$, for the relative error in the truncation of the collision operator given by (24), as a function of v and g_{tr}. For this contour plot we have used the Maxwellian upper bound given by Method I. The results obtained with Method II are quite similar: For each v the contours are shifted up or down by about 0.5 in g_{tr}. The contour plot shows that if we choose $g_{\mathrm{tr}} = 6$ then $\mathcal{E}_{\mathrm{rel}} < 10^{-1}$ for $v \leq 4$, which corresponds to probabilities down to a level of 2×10^{-5} for the limiting Maxwellian pdf. Similarly, if $g_{\mathrm{tr}} = 8$ then $\mathcal{E}_{\mathrm{rel}} < 10^{-1}$ for $v \leq 6$, corresponding to probabilities down to 10^{-9}. In this manner, the results in Fig. 2 can be used to select a value of g_{tr} that is small but that nevertheless guarantees a desired accuracy for the approximation $Q^{\mathrm{tr}} \approx Q$. The advantage of choosing smaller values for g_{tr} is that we can then choose smaller values for L and N, thereby reducing the computational cost, which is $\mathcal{O}(N^6)$.

In Fig. 2 (right) we plot slices of $\mathcal{E}_{\mathrm{rel}}(v, g_{\mathrm{tr}})$ for three values of v. The colored solid curves with symbols show the results obtained with Theorem 1, while the black dashed curves show the corresponding results obtained using (1). Even with $k = 0.5$, the asymptotic formulae (33) agree extremely well with (24), except when g_{tr} is slightly larger than v. These plots confirm that once $g_{\mathrm{tr}} > v$, $Q^{\mathrm{tr}}(\mathbf{v}) \to Q(\mathbf{v})$ exponentially fast as $g_{\mathrm{tr}} \to \infty$. However, the pointwise nature of the convergence is obvious in the plots.

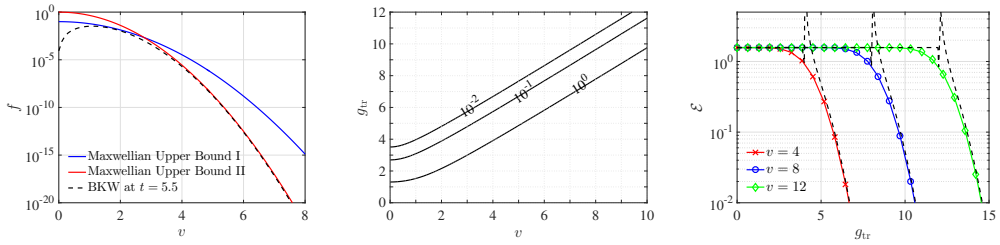

Figure 2: Left: Log-scale plot of the initial BKW velocity pdf given by (17) at the initial time, $t = 5.5$, (dashed black curve), together with the Maxwellian upper bounds obtained using Method I (solid blue curve) and Method II (solid red curve). Middle: Contour plot of the upper bound, $\mathcal{E}_{\rm rel}$, for the relative error in the truncation of the collision operator given by (24), as a function of speed, v, and truncation parameter, $g_{\rm tr}$. This result was obtained using the Maxwellian upper bound obtained using Method I. Right: Slices of $\mathcal{E}_{\rm rel}(v, g_{\rm tr})$ for three values of v. The colored solid curves with symbols show the results obtained with (24) and the black dashed curves show the corresponding asymptotic formulae in (33).

In Fig. 3 we assess the accuracy of the numerical computation of $Q^{\rm tr}$ by plotting the maximum of the total error, $\mathcal{E}_{\rm tot}$ in (19), as a function of speed v, for several different choice of $g_{\rm tr}$ and N. Here, the maximum is taken over all $\mathbf{v}$ with $|\mathbf{v}| = v$. In the top left panel, we show the results with $g_{\rm tr} = 6$. Using solid colored curves with symbols we plot $\max(\mathcal{E}_{\rm tot})$ for $N = 24$ (blue curve with circles), $N = 36$ (black curve with crosses), $N = 48$ (red curve with pluses), and $N = 72$ (magenta curve with diamonds). We also plot the collision operator, Q, obtained analytically from (4) and (17) (dashed black curve) and the upper bound, $\mathcal{E}_{\rm tr}^{\rm UB}$ in (23), for the truncation error (solid black curve). Because these two curves intersect at $v = 4$, we can only be guaranteed that $|Q^{\rm tr} - Q| < |Q|$ for $v \leq 4$. For each N, the numerically computed collision operator, $Q^{\rm NC}$, is an accurate approximation to Q in the interval where the solid curve with symbols lies below the black dashed curve. The reason this interval extends past $v = 4$ for $N \geq 48$ is that the upper bound $\mathcal{E}_{\rm tr}^{\rm UB}$ for $|Q^{\rm tr} - Q|$ is not optimal. In the top right panel, we show the corresponding results with $g_{\rm tr} = 8$. Because the solid black and dashed black curves intersect at $v = 5$, we are guaranteed that if we choose N to be sufficiently large, then the solution will be accurate out to at least $v = 5$. Clearly, the choice $N = 48$ is not large enough. However, if we choose $N = 72$, corresponding to a 12-fold increase in the computational time, then the solution is accurate out to $v = 6$. In the bottom left panel for which $g_{\rm tr} = 12$, the solid black curve is not visible since $\mathcal{E}_{\rm tr}^{\rm UB} < 10^{-15}$. However,

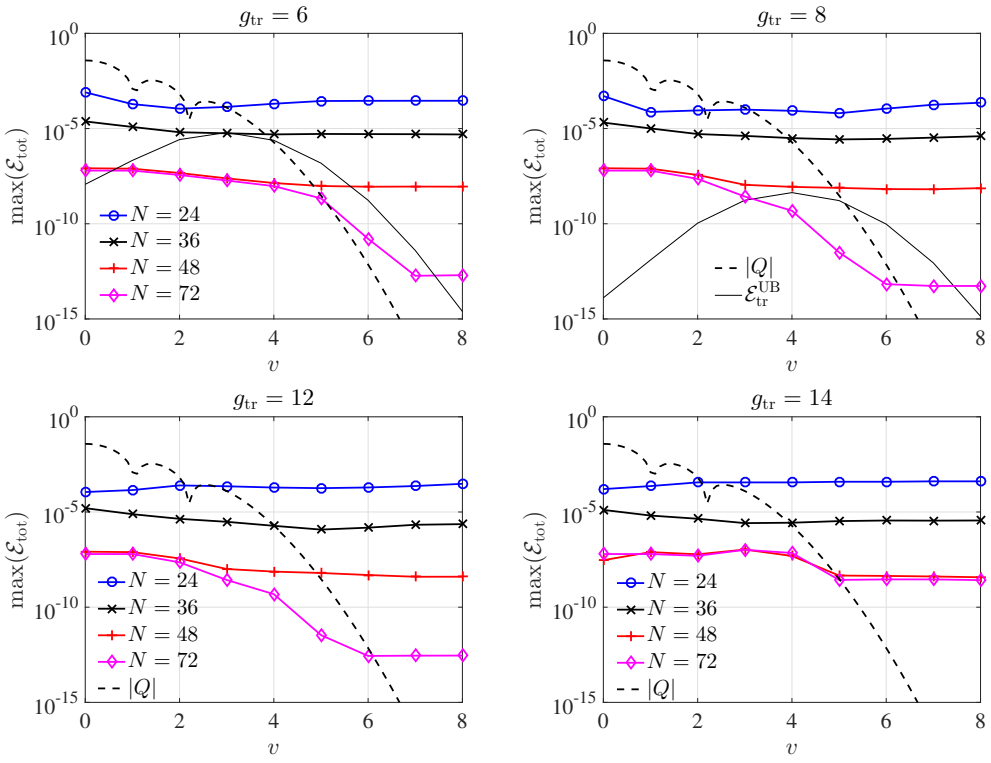

Figure 3: Maximum of the total error, $\mathcal{E}_{\rm tot}$ in (19), as a function of speed v, for several different choices of $g_{\rm tr}$ and N. These results are for the BKW solution. Here, the maximum is taken over all $\mathbf{v}$ with $|\mathbf{v}| = v$. The solid colored curves with symbols show plots of $\max(\mathcal{E}_{\rm tot})$ for the values of N shown in the legend. The black dashed curve shows the collision operator, Q, obtained from (4) and (17), and the solid black curve shows the upper bound, $\mathcal{E}_{\rm tr}^{\rm UB}$ in (23), for the truncation error.

there is no change in the $\mathcal{E}_{\rm tot}$-curves compared to the case that $g_{\rm tr} = 8$, since the total error is dominated by the error in the numerical computation of $Q^{\rm tr}$. Finally, in the bottom right panel with $g_{\rm tr} = 14$, we see that there is no advantage to increasing N from 48 to 72 since that does not decrease $\Delta\xi$ and the convolution weighting function, $\widehat{G}^{\rm tr}$, now oscillates too rapidly. This last result is in accord with the large jump in the errors from $g_{\rm tr} = 12$ to $g_{\rm tr} = 16$ that we observed for the Maxwellian pdf in Table 1.

In the top row of Fig. 4, we plot $|Q|$ as a function of v_x at $(v_y, v_z) = (0, 0)$. We show the numerical results obtained with $g_{\rm tr} = 8$ (left) and $g_{\rm tr} = 14$ (right) for the values of N shown in the legend. We also show the analytical

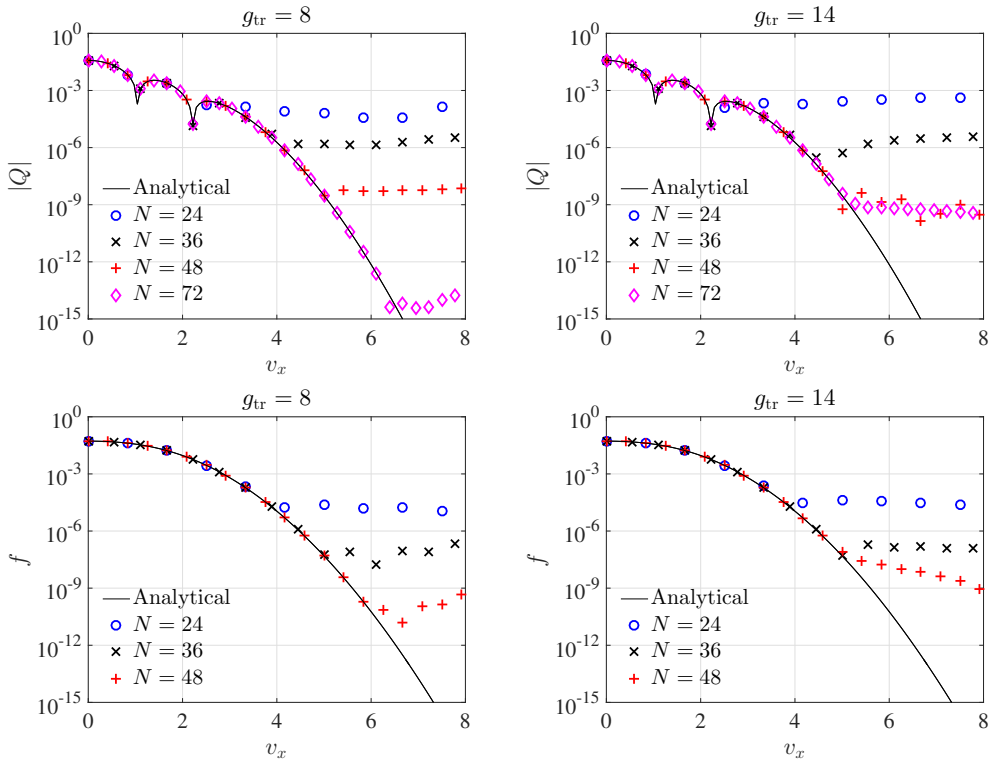

Figure 4: Collision operator at $t = 5.5$ (top row) and velocity pdf at $t = 9$ (bottom row) for the BKW solution. The numerical results were obtained with $g_{\rm tr} = 8$ (left column) and $g_{\rm tr} = 14$ (right column) for the values of N shown in the legends. The analytical solutions are shown with the black solid curves.

result obtained from (4) and (17) with a black solid curve. The cusps correspond to the values of v_x for which $Q = 0$. On a linear scale (not shown), we obtain excellent agreement for all values of N. With $N = 48$, we obtain excellent agreement down to the level of less than 10^{-8}, and with $N = 72$ down to 10^{-14}. The results with $g_{\rm tr} = 6$, 10, and 12 (not shown) are only slightly worse than with $g_{\rm tr} = 8$. However, just as in Fig. 3, with $g_{\rm tr} = 14$ we cannot reduce the error level below 10^{-9}. In the bottom row, we plot the velocity pdf at $t = 9$, using the same format as in the top row. For these results we solved (4) using Euler's method with a time step of $\Delta t = 0.05$. However, we did not perform the computation with $N = 72$ as the computational cost was prohibitive.

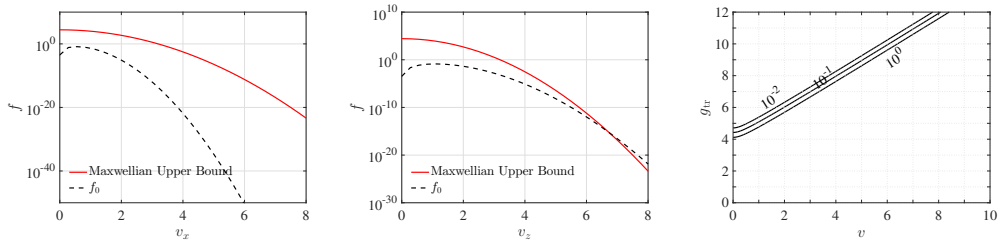

Figure 5: Left and Middle: Log-scale plot of the cylindrically symmetric initial velocity pdf (41) (dashed black curve) and the Maxwellian upper bound (solid red curve) as functions of v_x when $(v_y, v_z) = (0, 0)$ (left) and v_z when $(v_x, v_y) = (0, 0)$ (middle). Right: Contour plot of the upper bound, $\mathcal{E}_{\rm rel}$, for the relative error in the truncation of the collision operator given by (24), as a function of speed, v, and truncation parameter, $g_{\rm tr}$.

6.3. A cylindrically symmetric initial condition

In this subsection, we apply the spectral method to solve the homogeneous Boltzmann equation (4) in the case that the initial condition is the cylindrically symmetric velocity pdf,

$$f_{\rm cyl}(0, \boldsymbol{v}) \;=\; A\left[\tfrac{5K-3}{K} + \tfrac{1-K}{K^2}\left(c^2v_x^2 + c^2v_y^2 + v_z^2\right)\right]\exp\left[-(c^2v_x^2 + c^2v_y^2 + v_z^2)/2K\right], \tag{41}$$

obtained by dilating the BKW initial condition (17) by a factor, $1/c$, in the v_x and v_y-dimensions. As in Section 6.2, we choose $K = 1 - e^{-5.5/6}$. We choose the dilation constant to be $c = 2$ and we choose the constant, A, so that the pdf integrates to 1.

In Fig. 5, we plot the initial pdf, $f_{\rm cyl}$, and the Maxwellian upper bound obtained using Method I, which gives $k = 0.9$ and $c = 1.5 \times 10^5$. We plot these pdfs as a function of both v_x when $(v_y, v_z) = (0, 0)$ (left) and v_z when $(v_x, v_y) = (0, 0)$ (middle). In the right panel, we show a contour plot of the bound, $\mathcal{E}_{\rm rel}$, for the relative error in the truncation of the collision operator given by (24), as a function of v and $g_{\rm tr}$. We observe that the contours are translated up by about 2 compared to the ones in Fig. 2. The contour plot shows that if we choose $g_{\rm tr} = 10$ then $\mathcal{E}_{\rm rel} < 10^{-1}$ for $v \le 6$.

In the top row of Fig. 6, we plot the numerical collision operator as a function of v_x (left) and v_z (right). These results were obtained using $N = 72$ for the values of $g_{\rm tr}$ shown in the legend. The results for $g_{\rm tr} = 4$ and 16 are less accurate than those for $g_{\rm tr} = 8$ and 12. The results for $g_{\rm tr} = 4$ is consistent with the contour plot in Fig. 5, which shows that the truncation error is too large when $g_{\rm tr} = 4$. Because of the more rapid decay of the

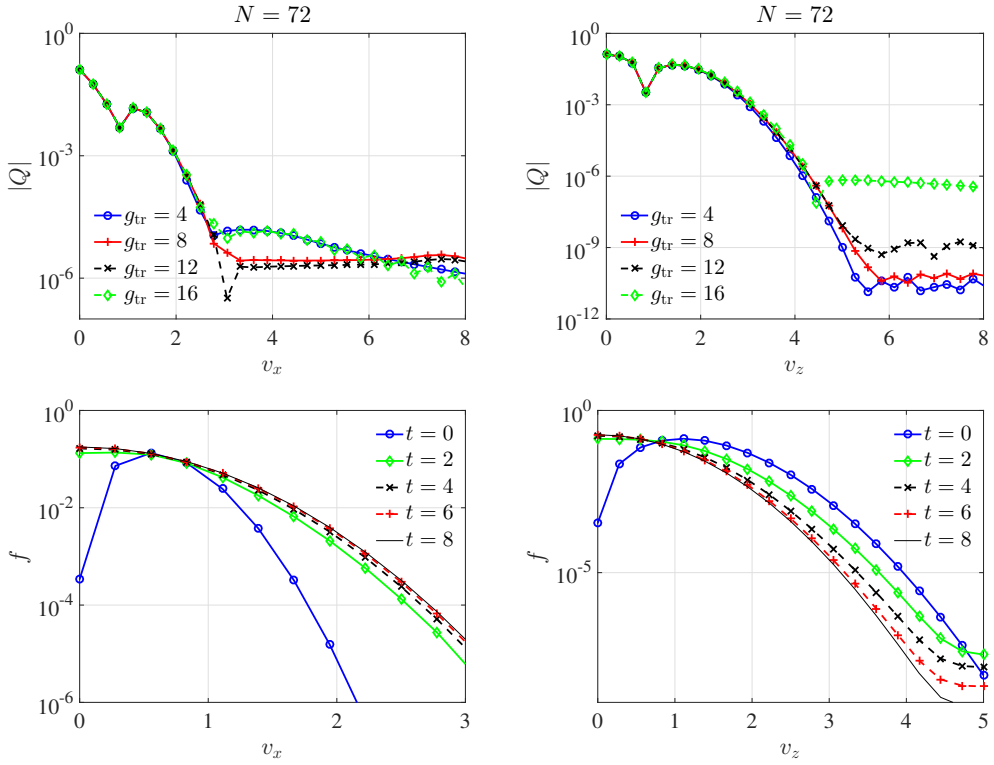

Figure 6: Top row: Collision operator at $t = 5.5$ as a function of v_x (left) and v_z (right) for the cylindrically symmetric initial velocity pdf (41) with $c = 2$ and $N = 72$, for the values of $g_{\rm tr}$ shown in the legends. Bottom row: The corresponding velocity pdfs at the times shown in the legends, computed using $g_{\rm tr} = 12$.

cylindrically symmetric initial condition in the v_x-direction, the error in the numerical computation of $Q^{\rm tr}$ is the dominant source of error with $g_{\rm tr} = 8$ and 12. In the bottom row of Fig. 6, we plot the evolution of the velocity pdf over the time interval $[0, 8]$. These results were obtained with $g_{\rm tr} = 12$, using the Adams-Bashforth method (40) with $\Delta t = 0.125$. We verified that the number density, momentum, and energy are preserved up to round-off error. The pdf at $t = 8$ agrees well with the equilibrium Maxwellian pdf (not shown) over the range of probability values in the plots. The plots show the rates at which the velocity pdf converges to the equilibrium pdf in the different velocity dimensions.

6.4. Mixture of Maxwellians initial conditions

For the next two examples, we suppose that the initial velocity pdf is a mixture of Maxwellian pdfs of the form

$$f_{\text{mix}}(\boldsymbol{v}) \;=\; \omega f(\boldsymbol{v}-\boldsymbol{v}_1, T_1) \;+\; (1-\omega) f(\boldsymbol{v}-\boldsymbol{v}_2, T_2), \tag{42}$$

where $f(\boldsymbol{v}, T) = (2\pi T)^{-3/2} \exp(-v^2/2T)$.

For our first example, we chose $\omega = 0.5$, $\boldsymbol{v}_1 = (2,0,0)$, $\boldsymbol{v}_2 = -\boldsymbol{v}_1$, and $T_1 = T_2 = 0.25$. In Fig. 7, we plot the initial pdf, f_{mix}, and the Maxwellian upper bound obtained using Method I, which gives $k = 0.32$ and $c = 1.1$. We plot these pdfs as a function of both v_x when $(v_y, v_z) = (0,0)$ (left) and v_y when $(v_x, v_z) = (0,0)$ (middle). In the right panel, we show a contour plot of the bound, $\mathcal{E}_{\text{rel}}$, for the relative error in the truncation of the collision operator given by (24), as a function of v and g_{tr}. Guided by this contour plot, for the computation of the velocity pdf we chose $g_{\text{tr}} = 10$ to ensure that $\mathcal{E}_{\text{rel}} < 10^{-1}$ for $v \le 6$.

In Fig. 8, we show the evolution of the velocity pdf on a linear scale (left column) and logarithmic scale (right column), plotted as a function of v_x (top row) and v_z (bottom row). These results were obtained with $N = 84$ and $\Delta t = 0.2$. We verified our results by comparison to analytic formulae for the moments of the velocity pdf [12]. The relative errors in the pressure and scalar fourth-order moment were less than 2×10^{-4} and the absolute error in the heat flux was less than 4×10^{-6}. From $t = 0$ to $t = 3$, we observe a rapid increase in the very low initial probability of high speed particles in the v_z-direction. Over the same time period, there is a substantial decay in the peaks of the initial pdf at $\boldsymbol{v} = \boldsymbol{v}_1$ and $\boldsymbol{v} = \boldsymbol{v}_2$. At $t = 15$ the agreement with the limiting Maxwellian pdf is excellent down to a probability level of 10^{-10}, i.e., $v < 8$. However, on a logarithmic scale, when $v > 6$ we observe what appear to be numerical artifacts in the velocity pdf at $t = 3$.

For our second example, we chose $\omega = 0.9999$, $\boldsymbol{v}_1 = (0,0,0)$, $\boldsymbol{v}_2 = (7.38,0,0)$, $T_1 = 4$ and $T_2 = 0.0625$. With these parameters, the initial pdf is a perturbation of a Maxwellian pdf which has a small bump centered at $\boldsymbol{v} = \boldsymbol{v}_2$ whose amplitude is 0.05 of that of the dominant Maxwellian, and which is located where the dominant Maxwellian has a probability density of 10^{-5}. Since the probability mass of the bump is negligible, we used the dominant Maxwellian rather than the upper bound of Method I to estimate the relative error in the truncation of the collision operator. The resulting contour plot (not pictured) shows that we should choose $g_{\text{tr}} = 10$ to ensure that

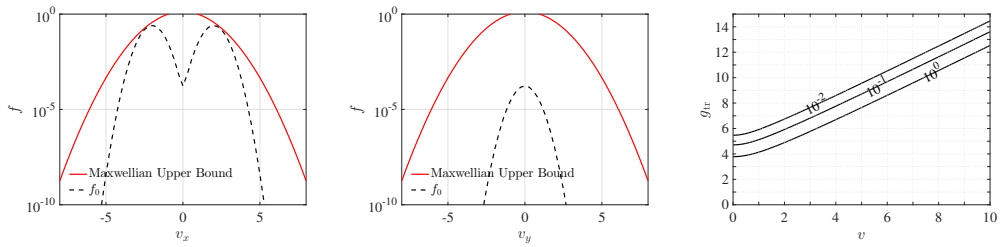

Figure 7: Left and Middle: Log-scale plot of the mixture of Maxwellians initial velocity pdf (42) (dashed black curve) and the Maxwellian upper bound (solid red curve) as functions of v_x when $(v_y, v_z) = (0, 0)$ (left) and v_y when $(v_x, v_z) = (0, 0)$ (right). The parameters in (42) were chosen to be $\omega = 0.5$, $\boldsymbol{v}_1 = (2, 0, 0)$, $\boldsymbol{v}_2 = -\boldsymbol{v}_1$, and $T_1 = T_2 = 0.25$. Right: Contour plot of the upper bound, $\mathcal{E}_{\text{rel}}$, for the relative error in the truncation of the collision operator given by (24).

$\mathcal{E}_{\text{rel}} < 10^{-1}$ for $v \leq 8$. As in the previous simulation, we also chose $N = 84$ and $\Delta t = 0.2$. The relative error in the pressure was less than 4×10^{-4} while that of the scalar fourth-order moment was less than 6×10^{-2}. The absolute error in the heat flux was less than 5×10^{-2}. In Fig. 9, we plot the velocity pdf at the times shown in the legends as a function of v_x for $(v_y, v_z) = (0, 0)$ on a linear scale (left) and logarithmic scale (right). This simulation result shows the rate at which this localized, low-amplitude perturbation of a Maxwellian pdf relaxes back to the limiting Maxwellian. Because of how we chose g_{tr}, the gradual growth of the pdf where $v > 8.5$ is likely due to errors in the numerical computation of the collision operator. At all times, the slices of the pdf at $(v_x, v_z) = (0, 0)$ and $(v_x, v_y) = (0, 0)$ (not shown) are visually indistinguishable from the dominant Maxwellian.

6.5. Results for a simple plasma model

For our final example, we consider a spatially homogeneous model for the velocity pdf of the electrons in a simplified plasma system that includes an electron gun source, electron-electron collisions, and loss of high velocity electrons into a wall. We model this system using the equation

$$\frac{\partial f}{\partial t}(t, \mathbf{v}) \;=\; Q(f, f)(t, \mathbf{v}) \;+\; c_S S(\mathbf{v}) \;-\; c_L L(\mathbf{v}) f(t, \mathbf{v}), \tag{43}$$

where the electron gun source is modeled by $S(\mathbf{v}) = \exp(\|\mathbf{v} - \mathbf{v}_S\|^2 / 2\sigma_S^2)$ with $\mathbf{v}_S = (2, 0, 0)$ and $\sigma_S = 0.25$, and the loss is given by $L(\mathbf{v}) = \frac{-1}{\pi} \arctan[(v_x -$

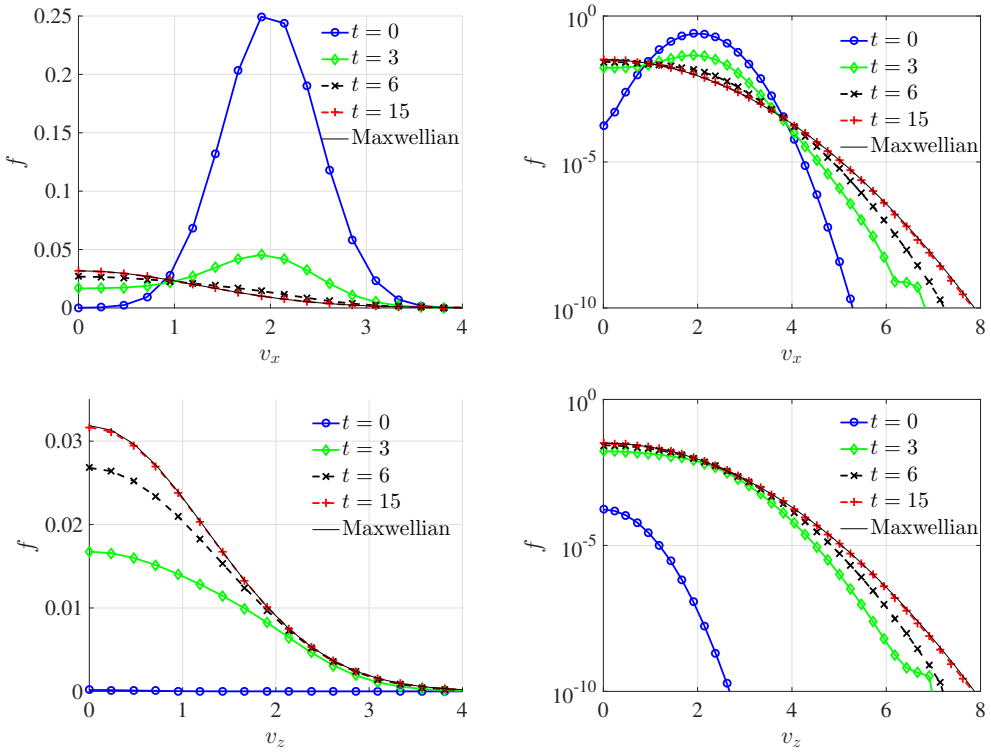

Figure 8: Velocity pdf on a linear scale (left column) and logarithmic scale (right column), plotted as a function of v_x (top row) and v_z (bottom row) at the times shown in the legends for the initial condition in Fig. 7. The limiting Maxwellian pdf is shown with the thin solid black curve.

$v_L)/\sigma_L] + \frac{1}{2}$ with $v_L = -2$ and $\sigma_L = 10^{-6}$. This loss function models absorption of particles moving at high speed towards a wall parallel to the yz-plane. To approximately balance gain and loss, we chose the coefficients in (43) to be $c_S = 0.1$ and $c_L = 10$. For these simulations we chose $g_{\text{tr}} = 10$, $N = 80$, and $\Delta t = 0.02$. The small value of Δt was chosen to ensure that the numerical solution did not become negative due to the presence of the loss term. The initial velocity pdf was chosen to be a Maxwellian with temperature $T = 1$.

In Fig. 10, we plot the time evolution of the velocity pdf as a function of v_x. As time increases from $t = 0$ to $t = 36$, the number density, energy, and the x-component of the momentum all increase due to the source, and the tail of the pdf in the negative v_x-direction deviates significantly from that of a Maxwellian distribution due to the loss term. In addition, the pdf is highly

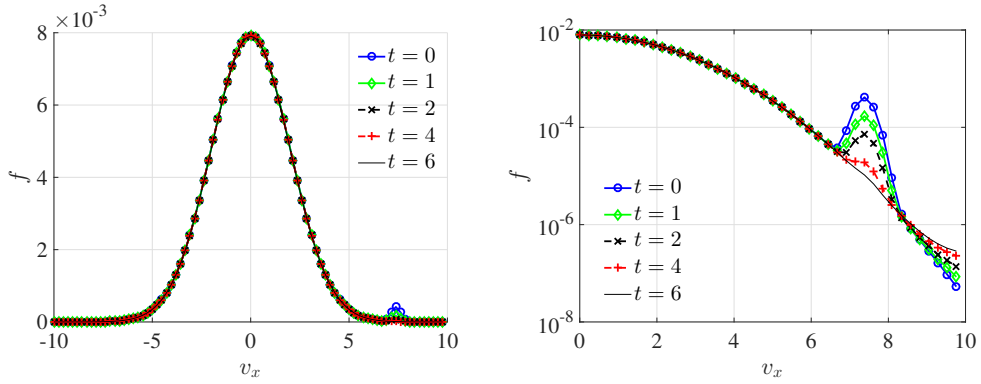

Figure 9: Velocity pdf on a linear scale (left) and logarithmic scale (right), plotted as a function of v_x at the times shown in the legends. The parameters in (42) were chosen to be $\omega = 0.9999$, $\boldsymbol{v}_1 = (0, 0, 0)$, $\boldsymbol{v}_2 = (7.38, 0, 0)$, $T_1 = 4$, and $T_2 = 0.0625$.

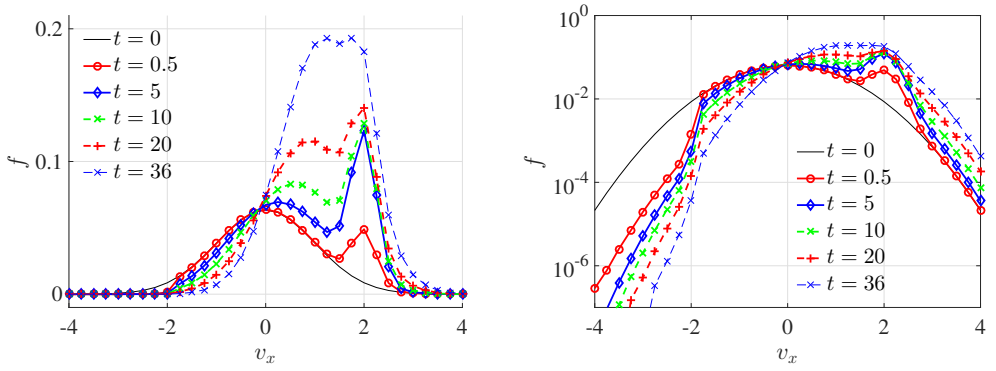

Figure 10: Velocity pdf for the simple plasma system modeled by (43) at the times shown in the legends. The pdf is plotted as a function of v_x at $(v_y, v_z) = (0, 0)$ on a linear scale (left) and a logarithmic scale (right).

asymmetric in the v_x-dimension due to the combined effects of the source and loss terms.

7. Conclusions

We have demonstrated the feasibility of using the spectral-Lagrangian method of Gamba and Tharkabhushanam to compute the velocity pdf of a particle species well into the low-probability tails. Calculation of the high-energy tails out to at least three standard deviations could enable improve-

ments to be made in the modeling of chemical reactions and ionization events in low-temperature, industrial plasmas. Although other researchers [23, 22] have reported low L^2-errors in numerical computation of the effect that particle collisions have on the distribution of particle velocities, the results presented here are the first we know of that explicitly study the accuracy of the deterministic computation of the low-probability tails.

To obtain these results, we examined the critical role that the truncation parameter, $g_{\rm tr}$, plays in the accuracy of the numerical computation of the collision operator. Although there is a theoretical guarantee that the truncated collision operator, $Q^{\rm tr}$, converges to Q as $g_{\rm tr} \to \infty$, this result is based on the assumption that the weighted convolution integral defining $Q^{\rm tr}$ can be computed exactly without numerical error. However, we demonstrated that if $g_{\rm tr}$ is too large then accurate numerical computation of the weighted convolution integral is not feasible since the decay rate and degree of oscillation of the convolution weighting function both increase as $g_{\rm tr}$ increases. As a consequence, in practice we are forced to examine the trade off between the error inherent in the truncation of the collision operator and the error in the numerical computation of the truncated operator. To do so, we derived an upper bound on the pointwise error between $Q^{\rm tr}$ and Q, assuming that both operators are computed exactly. Unlike in the previous formula for $g_{\rm tr}$ given by Gamba and Tharkabhushanam [13], to obtain this bound we only needed to assume that the velocity pdf is bounded above by a Maxwellian pdf, rather than being compactly supported. We then showed how to use this bound to guide the choice of $g_{\rm tr}$ in numerical computations of the low-probability tails of the velocity pdf. Finally, although our numerical results were obtained in the spatially homogeneous case, the error estimate we derived could also be used to guide the choice of $g_{\rm tr}$ for the computation of spatially inhomogeneous velocity pdfs, since the collision operator is independently computed at each spatial position, and, if necessary, the truncation parameter, $g_{\rm tr}$, can be chosen to be spatially dependent.

Acknowledgements. We thank Jeff Haack for helpful conversations.

References

[1] B. Gustavsson, T. Sergienko, I. Häggström, F. Honary, T. Aso, Simulation of high energy tail of electron distribution function, Adv. Polar Upper Atmos. Res. 18 (2004) 1–9.

[2] J. Allen, On the applicability of the Druyvesteyn method of measuring electron energy distributions, Journal of Physics D: Applied Physics 11 (3) (1978) L35.

[3] J. V. Dicarlo, M. J. Kushner, Solving the spatially dependent Boltzmann's equation for the electron velocity distribution using flux corrected transport, J. Appl. Phys. 66 (12) (1989) 5763–5774.

[4] T. Sheridan, M. Goeckner, J. Goree, Electron velocity distribution functions in a sputtering magnetron discharge for the E ×B direction, Journal of Vacuum Science & Technology A: Vacuum, Surfaces, and Films 16 (4) (1998) 2173–2176.

[5] C. Sozzi, E. De La Luna, D. Farina, J. Fessey, L. Figini *et al.*, Measurement of electron velocity distribution function, AIP Conference Proceedings 988 (73) (2008) 73–80.

[6] W. Tan, Langmuir probe measurement of electron temperature in a Druyvesteyn electron plasma, Journal of Physics D: Applied Physics 6 (10) (1973) 1206.

[7] J. Poulose, M. Goeckner, S. Shannon, D. Coumou, L. Overzet, Driving frequency fluctuations in pulsed capacitively coupled plasmas, The European Physical Journal D 71 (9) (2017) 242.

[8] A. G. Bird, Molecular Gas Dynamics, Clarendon Press, Oxford, 1994.

[9] K. Nanbu, Direct simulation scheme derived from the Boltzmann equation. I. Monocomponent gases, J. Phys. Soc. Japan 52 (1983) 2042–2049.

[10] W. Wagner, A convergence proof for Bird's direct simulation Monte Carlo method for the Boltzmann equation, Journal of Statistical Physics 66 (3) (1992) 1011–1044.

[11] I. M. Gamba, S. Rjasanow, W. Wagner, Direct simulation of the uniformly heated granular Boltzmann equation, Mathematical and Computer Modeling 42 (5-6) (2005) 683–700.

[12] S. Rjasanow, W. Wagner, Stochastic Numerics for the Boltzmann Equation, Springer, Berlin, 2005.

[13] I. M. Gamba, S. H. Tharkabhushanam, Spectral-Lagrangian methods for collisional models of non-equilibrium statistical states, Journal of Computational Physics 228 (2009) 2012–2036.

[14] C. Mouhot, L. Pareschi, Fast algorithm for computing the Boltzmann collision operator, Math. Comp. 75 (256) (2006) 1833–1852.

[15] L. Pareschi, B. Perthame, A Fourier spectral method for homogeneous Boltzmann equations, Transport Theory and Statistical Physics 25 (3-5) (1996) 369–382.

[16] L. Pareschi, G. Russo, Numerical solution of the Boltzmann equation. I. Spectrally accurate approximation of the collision operator, SIAM J. Numerical Anal. 37 (4) (2000) 1217–1245.

[17] I. M. Gamba, J. R. Haack, A conservative spectral method for the Boltzmann equation with anisotropic scattering and the grazing collisions limit, Journal of Computational Physics 270 (2014) 40–57.

[18] I. M. Gamba, J. R. Haack, C. D. Hauck, J. Hu, A fast spectral method for the Boltzmann collision operator with general collision kernels, SIAM Journal on Scientific Computing 39 (4) (2017) B658–B674.

[19] I. M. Gamba, S. H. Tharkabhushanam, Shock and boundary structure formation by spectral-Lagrangian methods for the inhomogenerous Boltzmann transport equation, Journal of Computational Mathematics 28 (2010) 430–460.

[20] J. R. Haack, I. M. Gamba, High performance computing with a conservative spectral Boltzmann solver, in: AIP Conference Proceedings, Vol. 1501, AIP, 2012, pp. 334–341.

[21] A. Munafò, J. R. Haack, I. M. Gamba, T. E. Magin, A spectral-Lagrangian Boltzmann solver for a multi-energy level gas, Journal of Computational Physics 264 (2014) 152–176.

[22] I. M. Gamba, S. Rjasanow, Galerkin-Petrov approach for the Boltzmann equation, Journal of Computational Physics 366 (2018) 341–365.

[23] E. Fonn, P. Grohs, R. Hiptmair, Hyperbolic cross approximation for the spatially homogeneous Boltzmann equation, IMA Journal of Numerical Analysis 35 (4) (2014) 1533–1567.

[24] Z. Cai, Y. Fan, L. Ying, An entropic Fourier method for the Boltzmann equation, SIAM Journal on Scientific Computing 40 (5) (2018) A2858–A2882.

[25] I. M. Gamba, J. R. Haack, J. Hu, A fast conservative spectral solver for the nonlinear Boltzmann collision operator, in: AIP Conference Proceedings, Vol. 1628, AIP, 2014, pp. 1003–1008.

[26] R. Alonso, I. Gamba, S. Tharkabhushanam, Convergence and error estimates for the Lagrangian-based conservative spectral method for Boltzmann equations, SIAM Journal on Numerical Analysis 56 (6) (2018) 3534–3579.

[27] C. Cercignani, R. Illner, M. Pulvirenti, The mathematical theory of dilute gases, Vol. 106, Springer Science & Business Media, 2013.

[28] J. Haack, A hybrid OpenMP and MPI implementation of a conservative spectral method for the Boltzmann equation, ArXiv e-prints`http://adsabs.harvard.edu/abs/2013arXiv1301.4195H` (Jan 2013).

[29] J. Duistermaat, J. Kolk, Distributions: Theory and Applications, Springer, New York, 2010.

[30] A. Bobylev, Exact solutions of the Boltzmann equation, in: Akademiia Nauk SSSR Doklady, Vol. 225, 1975, pp. 1296–1299.

[31] K. Max, W. T. Tsun, Formation of Maxwellian tails, Physical Review Letters 36 (1976) 1107–1109.

[32] A. V. Bobylev, S. Rjasanow, Difference scheme for the Boltzmann equation based on the fast Fourier transform, European Journal of Mechanics - B/Fluids 16 (2) (1997) 869–887.

[33] A. Bobylev, I. Gamba, Upper Maxwellian bounds for the Boltzmann equation with pseudo-Maxwell molecules, Kinet. Relat. Models 10 (3) (2017) 573–585.

[34] I. Gamba, V. Panferov, C. Villani, Upper Maxwellian bounds for the spatially homogeneous Boltzmann equation, Arch. Rat. Mech. Anal. 194 (2009).

[35] N. Bleistein, R. A. Handelsman, Asymptotic expansions of integrals, Courier Corporation, 1986.

[36] L. N. Trefethen, Spectral Methods in MATLAB, SIAM, 2000.

[37] D. R. Kincaid, E. W. Cheney, Numerical Analysis: Mathematics of Scientific Computing, Wadsworth, Inc, Belmont, California, 1991.